

Published in final edited form as:

*ACS Nano*. 2011 July 26; 5(7): 5717–5728. doi:10.1021/nn2013904.

## The Impact of Silica Nanoparticle Design on Cellular Toxicity and Hemolytic Activity

Tian Yu<sup>1,3</sup>, Alexander Malugin<sup>1,3</sup>, and Hamidreza Ghandehari<sup>1,2,3,\*</sup>

<sup>1</sup>Department of Pharmaceutics and Pharmaceutical Chemistry, Nano Institute of Utah, University of Utah, Salt Lake City, Utah, 84108, U.S.A.

<sup>2</sup>Department of Bioengineering, Nano Institute of Utah, University of Utah, Salt Lake City, Utah, 84108, U.S.A.

<sup>3</sup>Utah Center for Nanomedicine, Nano Institute of Utah, University of Utah, Salt Lake City, Utah, 84108, U.S.A.

### Abstract

Understanding the toxicity of silica nanoparticles (SiO<sub>2</sub>) on the cellular level is crucial for rational design of these nanomaterials for biomedical applications. Herein, we explore the impacts of geometry, porosity and surface charge of SiO<sub>2</sub> on cellular toxicity and hemolytic activity. Nonporous Stöber silica nanospheres (115 nm diameter), mesoporous silica nanospheres (120 nm diameter, aspect ratio 1), mesoporous silica nanorods with aspect ratio of 2, 4 and 8 (width by length 80 × 200 nm, 150 × 600 nm, 130 × 1000 nm) as well as their cationic counterparts were evaluated on macrophages, lung carcinoma cells, and human erythrocytes. It was shown that the toxicity of SiO<sub>2</sub> is cell-type dependent and that surface charge and pore size govern cellular toxicity. Using inductively coupled plasma mass spectrometry, the cellular association of SiO<sub>2</sub> was quantitated with the association amount increasing in the following order: mesoporous SiO<sub>2</sub> (aspect ratio 1, 2, 4, 8) < amine-modified mesoporous SiO<sub>2</sub> (aspect ratio 1, 2, 4, 8) < amine-modified nonporous Stöber SiO<sub>2</sub> < nonporous Stöber SiO<sub>2</sub>. Geometry did not seem to influence the extent of SiO<sub>2</sub> association at early or extended time points. The level of cellular association of the nanoparticles was directly linked to the extent of plasma membrane damage, suggesting a biological cause-and-effect relationship. Hemolysis assay showed that the hemolytic activity was porosity- and geometry- dependent for bare SiO<sub>2</sub> and surface charge-dependent for amine-modified SiO<sub>2</sub>. A good correlation between hemolytic activity and cellular association was found on a similar dosage basis. These results can provide useful guidelines for the rational design of SiO<sub>2</sub> in nanomedicine.

### Keywords

Silica; nanotoxicity; nanomedicine; silica nanorods; porous SiO<sub>2</sub>

Silica-based nanomaterials have attracted much attention in biomedical applications as cell markers, gene transfection agents, imaging moieties as well as drug carriers.<sup>1–5</sup> They possess a variety of unique properties, such as ease of synthesis, availability of surface modification, robust mechanical properties, and relatively inert chemical composition.<sup>6, 7</sup>

\*Corresponding author: Hamidreza Ghandehari, PhD, Utah Center for Nanomedicine, Nano Institute of Utah, University of Utah, Salt Lake City, Utah 84108, U.S.A. Phone: 801-587-1566. Fax: 801-585-0575. hamid.ghandehari@pharm.utah.edu.

Supporting Information Available: Supporting information (Supplemental Calculation 1, Supplemental Figures 1–5) is also available via the Internet at <http://pubs.acs.org>.

Synthetic strategies in template fabrication have further enabled the production of silica nanomaterials with distinct shape features, with increasing interest in their evaluation in biological systems.<sup>8–11</sup> Despite these advantages, the influence of physicochemical factors such as geometry, pore size and surface functional groups of SiO<sub>2</sub> still needs to be carefully examined for successful utility of these constructs in nanomedicine.<sup>12</sup>

Emerging literature suggests that nano- and microparticle shape can influence cellular uptake and biodistribution.<sup>13–15</sup> For example it has been reported that high-aspect-ratio cationic hydrogel particles (150 × 450 nm) were internalized by HeLa cells four times faster than corresponding low-aspect-ratio particles (200 × 200 nm).<sup>13</sup> Other reports suggest that uniform micro-sized polystyrene beads with elliptical disk shape, had a longer half-life in circulation than their spherical counterparts and less residence time in the liver.<sup>14</sup> We have previously demonstrated that PEGylated gold nanorods (10 × 45 nm, 1.13 mV) had less liver uptake, longer blood circulation half-life, and higher tumor accumulation than PEGylated gold nanospheres (50 nm, -27.1 mV) in orthotopic ovarian tumor xenograft mice.<sup>15</sup> In addition to geometry, porosity and surface functionality of nanoparticles are also critical factors that can influence the interaction of silica nanoparticles with biological systems.<sup>16–18</sup> Pore size of SiO<sub>2</sub> is a key factor in determining the adsorption capacity of proteins such as bovine serum albumin where the adsorption capacity was elevated as the pore size of SiO<sub>2</sub> increased.<sup>16</sup> Maurer-Jones et al. have demonstrated that 25 nm, nonporous SiO<sub>2</sub> had a greater impact on cells than 25 nm porous SiO<sub>2</sub> since the former possessed higher “cell-contactable reactive surface area” to perturb cell function.<sup>17</sup> Slowing et al. have reported that the uptake of mesoporous silica nanoparticles by cervical cancer cells could be elevated by surface functionalization with cationic functionalities or targeting moiety.<sup>18</sup> Despite these initial studies, there is a need for a systematic investigation of the interdependent roles of nanoparticle geometrical effect, porosity and surface functionality on cellular uptake and toxicity.<sup>19–21</sup> Such studies will enable the elucidation of predominant factors that determine the extent of toxicity, which will then provide practical guidance for rationally designing SiO<sub>2</sub> as biomedical devices with minimum adverse effects.

In this study, multiple physicochemical parameters of SiO<sub>2</sub> were evaluated for their effects on cellular toxicity and hemolytic activity. In order to compare the effect of pore size, mesoporous and nonporous spherical SiO<sub>2</sub> of the same diameter (ca. 110 nm) were synthesized and evaluated. To demonstrate the effect of geometrical feature (represented as aspect ratio, ratio of length over width), silica nanorods were produced with similar diameters along the short axis (around 100 nm) and different lengths along the long axis (approximately 200 nm, 600 nm, 1000 nm). SiO<sub>2</sub> of different porosities and aspect ratios were modified with primary amine silane groups to generate cationic charge which is dramatically different from the anionic charge of bare silica nanoparticle counterparts to assess the impact of surface charge. SiO<sub>2</sub> with the engineered physicochemical features as mentioned above were subject to a series of toxicity assays on two model cell lines, namely RAW 264.7 (a model macrophage commonly used to represent the physiological scavengers of foreign nanoparticles exposed to *in vivo* systems<sup>22</sup>) and A549 (the non-small-cell lung cancer epithelial cells). These cells were selected as model cells for potential targeted delivery of bioactive and imaging agents. We further characterized the hemolytic activity of SiO<sub>2</sub> as an initial step to evaluate *ex vivo* blood biocompatibility.

## RESULTS AND DISCUSSION

### Nanoparticle Synthesis and Characterization

Nonporous SiO<sub>2</sub><sup>23</sup> and mesoporous SiO<sub>2</sub> of different geometrical features were synthesized and characterized using transmission electron microscopy (TEM), X-ray diffraction (XRD) and nitrogen adsorption-desorption analysis for size, mesopore arrangement, surface area

and pore size measurement (Table 1). Mesoporous SiO<sub>2</sub> of different shapes were synthesized by a one-step condensation and aging method.<sup>19, 24–29</sup> In the first step, mesoporous SiO<sub>2</sub> was formed by condensation under dilute silica source and low surfactant concentration conditions with ammonium hydroxide as the base catalyst. The shape and polydispersity of SiO<sub>2</sub> was mainly controlled by molar composition of reaction agents<sup>24–28</sup> and stirring rate.<sup>29</sup> By changing the concentration of tetraethyl orthosilicate (TEOS), cetyltrimethylammonium bromide (CTAB) and aqueous ammonia, reaction stirring rate, mesoporous SiO<sub>2</sub> with targeted diameters (ca. 100 nm), lengths and aspect ratios (1, 2, 4, 8) were synthesized. In general, the width of mesoporous SiO<sub>2</sub> was controlled by adjusting the ammonia concentration in the reaction mixture<sup>19</sup> with larger width obtained at increased ammonia concentration, while the length of mesoporous SiO<sub>2</sub> increased with increased TEOS concentration, increased CTAB concentration, increased ammonia concentration and reduced stirring speed.<sup>28, 29</sup> In the second step, mesoporous silica nanoparticles were subject to autoclaving at 100 °C for 24 hours to promote silica matrix crosslinking and to enhance the stability of mesopore structure.<sup>30, 31</sup>

Evident from TEM image analysis (Figure 1), nonporous silica nanospheres (Stöber) and mesoporous silica nanospheres (Meso S) were 115 ± 13 nm and 120 ± 25 nm in diameter, respectively. Mesoporous silica nanorods were produced with distinctly different geometrical features. They possessed similar diameter as that of nanospheres (around 100 nm) yet the aspect ratios were different (mesoporous SiO<sub>2</sub> with aspect ratio 2, 4, 8 were abbreviated as AR2, AR4, and AR8, respectively). The aspect ratio distribution histogram showed that each type of mesoporous SiO<sub>2</sub> possessed distinct shape characteristics compared with any other type of mesoporous SiO<sub>2</sub> (Figure 1G), except AR2 and AR4 had certain portion of overlapped aspect ratios. However, they still possessed distinct geometrical features considering their dimensions were significantly different from each other along the short or long axes.

Figure 2A–D presents the nitrogen adsorption-desorption isotherms for mesoporous SiO<sub>2</sub> of different shapes. Mesoporous SiO<sub>2</sub> exhibited type IV isotherms, which were typical of a mesopore structure. The filling of mesopores occurred at relative pressure ( $P/P_0$ ) of 0.3 to 0.5. Each type of nanoparticles also exhibited an additional capillary condensation at high relative pressure ( $P/P_0 > 0.90$ ), which was characteristic of a high degree of textural porosity.<sup>19, 21</sup> Mesoporous SiO<sub>2</sub> possessed relatively high surface area (280 – 1190 m<sup>2</sup>/g) as calculated by the Brunauer-Emmet-Teller (BET) method (Table 1).<sup>19, 21</sup> The external surface areas of mesoporous SiO<sub>2</sub>, which referred to cell-contactable surface area, were calculated from the  $t$  plots of their N<sub>2</sub> adsorption isotherms (Table 1).<sup>32</sup> Different mesoporous nanoparticles displayed a narrow distribution of pore size which centered around 2.7–2.8 nm in diameter as determined by the Barrett-Joyner-Halenda (BJH) method (Table 1).<sup>19, 21</sup> Meso S possessed typical MCM-41 type mesopore arrangement as reflected by the distinct peaks (100, 110, 200, 210) in XRD measurement (Figure 2E), which was in a good agreement with its high resolution TEM image (Figure 1F) showing 2D-hexagonal mesopores in the close-packing structure for this type of SiO<sub>2</sub>.<sup>28</sup> The mesopore structure of Meso S was also well maintained post amine modification (Figure 2F). Therefore, Meso S was compared with nonporous Stöber nanoparticles to study the pore size effect on cellular toxicity and hemolytic activity.

The dynamic light scattering measurements showed that the Meso S tended to agglomerate to a higher extent (257.8 ± 0.9 nm) and was thus more polydisperse in size distribution than nonporous Stöber nanoparticles (148.0 ± 0.4 nm) (Table 2). Due to the method limitations, dynamic light scattering measurements are not applicable to mesoporous silica nanorod structure because such measurement model assumes spherical shape of nanoparticles in suspension.<sup>29</sup> Zeta potential measurements showed that Stöber nanoparticles were highly

negatively charged ( $-50.4 \pm 1.0$  mV), indicating a fairly stable suspension in aqueous medium.<sup>33</sup> Amine-modified Stöber (SA) nanoparticles had relatively lower positive zeta potential ( $17.0 \pm 0.7$  mV), which implied a moderate stability in aqueous suspension (Table 2).<sup>31</sup> Mesoporous SiO<sub>2</sub> were highly negatively charged ( $< -30$  mV) as bare nanoparticles and were all highly positively charged ( $> 30$  mV) post amine modification, which indicated a high stability within suspension (The amine-modified mesoporous nanospheres or nanorods with aspect ratio of 2, 4, 8 were abbreviated as MA, 2A, 4A and 8A).<sup>33</sup> The absence of carbon chain band (wavenumber 3000 – 2800) in FT-IR spectrum of surfactant-removed nanoparticles confirmed the complete removal of CTAB from the products by acidic ethanol extraction method (Supplemental Figure 1). The endpoint chromogenic Limulus Amebocyte Lysate (LAL) test (Lonza, Walkersville, MD) showed that there was no detectable gram negative endotoxin on any type of nanoparticles at 1 mg/mL (the detection limit was less than 0.1 EU/mL), which was the highest concentration of nanoparticles used in the *in vitro* and *ex vivo* studies.

### Acute Cytotoxicity

The ability of SiO<sub>2</sub> with the engineered physicochemical features to induce acute cellular toxicity response was tested on RAW 264.7 and A549 cells by WST-8 assay. Results demonstrated that toxicity of SiO<sub>2</sub> was highly cell-type and nanoparticle-concentration dependent (Figure 3). All types of SiO<sub>2</sub> at concentration as high as 500  $\mu$ g/mL did not affect the relative viability of A549 cells after 24 hours exposure. For RAW 264.7 macrophages, nonporous or mesoporous SiO<sub>2</sub> caused dramatic toxicity post 24 hour incubation, leaving only ca. 20–40% viable cells compared with controls, while amine-modified counterparts caused limited toxicity with approximately 64–85% relative viability (Figure 3A). Since bare SiO<sub>2</sub> showed higher cytotoxicity on RAW 264.7, doses that led to reduced toxicity (250  $\mu$ g/mL with ca. 70% viability) or non-toxicity (100  $\mu$ g/mL with ca. 100% viability) have been identified (Figure 3B) to be used in the following plasma membrane integrity assay or nanoparticle cellular association quantitation assay.

### Proliferation Inhibition

The ability of nanoparticles to inhibit cell proliferation was cell type dependent (Figure 4). Cancer epithelial cells were resistant to all types of nanoparticle treatment up to 500  $\mu$ g/mL post 72 hour exposure, and only cells treated with 2A and 8A at 1000  $\mu$ g/mL exhibited moderate toxicity response, resulting in 60–70% viable cells compared with controls (Figure 4A–B). For macrophages, the nanoparticle concentration that led to 50% inhibition on cell growth (IC<sub>50</sub>) ranged approximately from 50 to 100  $\mu$ g/mL post 3-day exposure for bare SiO<sub>2</sub> (Figure 4C) and the IC<sub>50</sub> of bare nonporous and mesoporous SiO<sub>2</sub> were not distinguishable from one another ( $p > 0.05$ ). Interestingly, the reduction of IC<sub>50</sub> was not observed for nanoparticles post amine modification. Instead, several fold increase in IC<sub>50</sub> was detected for amine-modified nanoparticles (Figure 4D, Table 3). For example, the IC<sub>50</sub> of AR4 and 4A were  $91.6 \pm 5.9$   $\mu$ g/mL and  $184.2 \pm 17.1$   $\mu$ g/mL, respectively and IC<sub>50</sub> of AR8 and 8A were  $73.7 \pm 17.0$   $\mu$ g/mL and  $224.9 \pm 28.2$   $\mu$ g/mL, respectively. Changes in cell morphology were observed in RAW 264.7 post nanoparticle exposure for 24 hours (Supplemental Figure 2) or 72 hours (Supplemental Figure 3). Reduced cell density and rounded cells were observed for bare SiO<sub>2</sub> treated macrophages while swollen vacuoles in cells were frequently observed in amine-modified SiO<sub>2</sub> treated macrophages.

To assess whether toxicity was due to soluble factors that were released from nanoparticles<sup>12</sup>, the toxicity assay was performed on the supernatant of nanoparticle stock aqueous suspension. Results showed that the supernatant did not affect the relative viability compared with controls (data not shown). To evaluate whether toxicity was due to adsorbed endotoxin on nanoparticles<sup>34</sup> that was below the detection limit of LAL assay ( $< 0.1$  EU/

mL), endotoxin from reference standard *E. coli* stock was added to make 0.1 EU/mL concentration in the 500  $\mu\text{g/mL}$  of nanoparticle suspension. Results showed that the relative viability post 24 hour incubation and  $\text{IC}_{50}$  of nanoparticles post 72 hour exposure were not changed in the presence of added endotoxin compared with nanoparticle treatment without addition of endotoxin (data not shown). These results support the fact that the toxicity of  $\text{SiO}_2$  was due to cellular interaction with nanoparticles themselves, rather than a product of degradation or any associated contaminants. In order to look into the cause for reduced toxicity of amine-modified  $\text{SiO}_2$ , we conducted inductively coupled plasma mass spectrometry (ICP-MS) analysis on cells treated with nanoparticles and the results are discussed in cellular association section.

### Plasma Membrane Integrity

Plasma membrane damage is an important aspect of cellular toxicity upon nanoparticle treatment. When cells have plasma membrane damage, the propidium iodide in the solution passively diffuses into the cytoplasm and binds with intracellular DNA or RNA. By quantitating the percentage of propidium iodide positive cells, one could deduce the percentage of cells experiencing plasma membrane damage in the total cell population.<sup>35</sup> The results show that the ability of nanoparticles (250  $\mu\text{g/mL}$ ) to compromise the integrity of plasma membrane after 24 hour incubation was cell type dependent (Figure 5). For cancer epithelial cells, the percentage of propidium iodide positive cells was less than 3% for all types of  $\text{SiO}_2$  treatment. For macrophages, Stöber nanoparticles caused plasma membrane damage in 53% of the cell population, while all mesoporous  $\text{SiO}_2$  selected for this study caused plasma membrane damage in 6–15% of RAW 264.7 cell population. Stöber nanoparticles caused the highest percentage of propidium iodide positive cells probably due to their high silanol density on the external surface that were accessible to cell membrane, which caused significantly higher cellular impact than mesoporous  $\text{SiO}_2$ .<sup>36</sup> Amine-modified mesoporous  $\text{SiO}_2$  generated higher extent of plasma membrane damage in ca. 38% of the cells than their bare mesoporous counterparts. Plasma membrane damage in cells was probably not due to the sedimentation of the nanoparticles, as this experiment was repeated with nanoparticles being added before cells were carefully plated on top of the nanoparticles and the observed results were very similar (Supplemental Figure 4). Combining the results above, it seems that porosity and surface charge are the major factors that determine the extent of plasma membrane damage in cells.

### Cellular Association

The amount of cellular associated  $\text{SiO}_2$ , which included internalized nanoparticles or nanoparticles adhering to the extracellular matrix, was quantitated by ICP-MS.<sup>19</sup> Results show a similar pattern of cellular association of  $\text{SiO}_2$  with macrophages and cancer epithelial cells. However, the amount of silicon associated with macrophages was 10–15 times higher than that of the cancer epithelial cells (Figure 6A–B). Nonporous Stöber nanoparticles led to much higher cellular association than mesoporous nanoparticles both on a particle mass basis and on a particle number basis (Table 4). The level of cellular association was also highest for Stöber nanoparticles among all types of  $\text{SiO}_2$  including the amine-modified counterparts SA. This observation was possibly due to the highest silanol density on the continuous external surface of Stöber nanoparticles, which was reflected by the highest magnitude of negative charge ( $-50$  mV) for these particles.<sup>36</sup> The formation of porous structure or modification with primary amine groups led to reduced silanol density on the external surface of the particles ( $-33$  mV to  $-39$  mV for mesoporous  $\text{SiO}_2$ ) or shielding of surface silanol by amine functionalities, which reduced the accessibility of silanol groups to cells and in turn decreased the level of cellular association.<sup>36</sup>

On the other hand, amine-modified mesoporous SiO<sub>2</sub> (32 mV – 40 mV) showed significantly higher cellular association than their bare mesoporous counterparts ( $p < 0.05$ ), which appeared to contradict the aforementioned phenomenon with SA (17 mV) and Stöber nanoparticles. This indicated that there could be a surface charge “threshold” (> 30 mV) above which the amine functionalities facilitated nanoparticle-cell interaction through electrostatic interaction of positively charged amine groups with negatively charged cell membrane. Whereas below the “threshold”, there were less surface amine groups available and they had electrostatic interaction with surface silanols and covered the sites of silanol,<sup>37</sup> which eventually reduced the level of cellular association.

Bare mesoporous SiO<sub>2</sub>, irrespective of their shape features, exhibited similar level but lowest amount of cellular associated silicon. For A549 cells, the level of cell associated silicon from mesoporous SiO<sub>2</sub> exposure was even below the detection limit of ICP-MS (< 0.1 µg/mL for silicon element). There was no significant difference in the level of cellular association among all types of mesoporous SiO<sub>2</sub> ( $p > 0.05$ ). There was also no significant difference in the cellular association among all mesoporous SiO<sub>2</sub> post amine modification on both cell lines ( $p > 0.05$ ), except that 8A had significantly higher cellular association than other amine-modified mesoporous SiO<sub>2</sub> on A549 cells ( $p < 0.001$ ). This suggests that the curvature of cationic SiO<sub>2</sub> could influence the wrapping by cell membrane and affect the cellular association with non-phagocytic cells.<sup>13</sup>

In order to test if porosity, geometry and surface modification can influence the cellular association at earlier time point, selected SiO<sub>2</sub> including Stöber, Meso S, AR8 and MA were incubated with RAW 264.7 cells for 1 hour and the level of cellular association was detected by ICP-MS. The experiment was done at 4 °C or 37 °C to differentiate the amount of membrane bound SiO<sub>2</sub> with that of internalized SiO<sub>2</sub>, as incubation at low temperature (4 °C) drastically reduces the energy-dependent internalization process in cells.<sup>38</sup> Considering that the viability of cells could be affected upon incubation at 4 °C which subsequently could influence the protein content recovered, the relative viability of cells post 70 minute incubation (10 minute pre-incubation and 60 minute incubation with nanoparticles) at 4 °C was measured and the results show that the percentage of viable cells was  $94 \pm 8\%$  compared with control cells treated at 37 °C for the same time duration. As shown in Figure 6C, Stöber nanoparticles led to a significant increase in cellular association 24 hours post incubation at 37 °C compared with 1 hour incubation at 37 °C ( $p < 0.001$ ) or at 4 °C ( $p < 0.001$ ), indicating that there was extensive internalization of nonporous nanoparticles over 24 hours. There was no significant difference in cellular association between Meso S and AR8 post 1 hour incubation at 37 °C ( $p > 0.05$ ). Geometry did not seem to affect the level of cellular associated nanoparticles for mesoporous SiO<sub>2</sub> at the early time point as well. Most mesoporous SiO<sub>2</sub> seemed to bind to the cell membrane instead of being internalized into the cytoplasm within an hour as the level of silicon association from Meso S or AR8 exposure was similar for cells incubated at 4 °C or 37 °C for one hour. However, the level of cellular association significantly increased post incubation for 24 hours compared with incubation for 1 hour at 37 °C for Meso S ( $p < 0.001$ ) and AR8 ( $p < 0.01$ ), which indicated that internalization of mesoporous SiO<sub>2</sub> had occurred. On the contrary, there was no significant difference in cellular association between 1 hour incubation and 24 hour incubation with MA at 37 °C ( $p > 0.05$ ), which implied that the cellular association of MA almost reached the plateau within 1 hour post incubation. The cellular association of MA post 1 hour incubation at 37 °C was not significantly higher than that at 4 °C ( $p > 0.05$ ). The combined results suggest that there was limited internalization over 24 hour post incubation with MA, which probably explained why there was a reduction in toxicity of amine-modified SiO<sub>2</sub> compared with that of bare SiO<sub>2</sub>. It has been suggested that the strong association of cationic SiO<sub>2</sub> with negatively charged cell membranes, which made the cationic SiO<sub>2</sub> adhere to cell membrane instead of bringing them into the cytoplasm, led to the reduction in

internalization and the resultant decreased toxicity based on transmission electron microscopy analysis<sup>39–41</sup> or confocal microscopy analysis<sup>42</sup>. Our results provide quantitative evidence by ICP-MS that there was limited internalization for amine-modified SiO<sub>2</sub>.

In summary, it appears that surface charge and porosity mainly influenced the extent of cellular association while geometry did not seem to influence cellular association within the aspect ratio range of 1–8 studied. These observations are consistent with the experiments examining plasma membrane integrity post nanoparticle treatment. The level of plasma membrane damage by nanoparticles was directly related to the extent of nanoparticle cellular association, which indicated a biological cause-and-effect relationship between cellular association and cell membrane damage on both cell lines.

## Hemolysis

The impact of nanoparticle porosity, geometry, and surface functionality on human red blood cells (RBCs) was evaluated by a hemolysis assay. The quantitation of hemoglobin in the supernatant of nanoparticle-RBC mixture was done by recording the absorbance of hemoglobin at 577 nm with a reference wavelength of 655 nm (Supplemental Figure 5).<sup>36, 43</sup> Results show that the extent of hemolysis was concentration-, porosity- and geometry-dependent for bare SiO<sub>2</sub> (Figure 7). Stöber nanoparticles caused an immediate onset of hemolysis that soon reached a plateau of 17% hemolysis at ca. 250 µg/mL probably due to its high negative charge which might expel RBCs (–15 mV)<sup>44</sup> from interacting at further increased nanoparticle concentration. For mesoporous SiO<sub>2</sub> of all geometries tested, no hemolytic toxicity was observed below 100 µg/mL. The impact of nanoparticle geometry became pronounced as the concentration further increased. Mesoporous SiO<sub>2</sub> with high aspect ratio demonstrated lower hemolytic activity than spherical or low aspect ratio mesoporous SiO<sub>2</sub>. It has been reported that the external surface area and the curvature of SiO<sub>2</sub> influence their hemolytic activity by affecting the magnitude of binding energy of particles with RBCs or bending energy of the membrane to wrap around nanoparticles.<sup>37</sup> Large external surface area and small curvature (i.e.  $1/r^2$  for spheres) rendered hemolysis process thermodynamically favorable.<sup>37</sup> In this case, the external surface areas of Stöber and Meso S were 24 and 109 m<sup>2</sup>/g, respectively, which agreed well with previous similar calculations,<sup>37, 43</sup> and had similar curvature due to the similar size they possessed. However, Meso S did not lead to a higher hemolytic rate than Stöber until the mass concentration exceeded beyond ca. 190 µg/mL. This indicates that there could possibly be a threshold in the density of silanol groups on each nanoparticle only above which it could cause immediate cell membrane damage upon exposure. Hence, the hemolytic activity depends not only on external surface area and curvature but also on silanol density of each nanoparticle exposed to RBCs.

The hemolytic activity of amine-modified SiO<sub>2</sub> was surface charge- and concentration-dependent (Figure 8). As the concentration increased, there was a rapid onset of hemolysis for all types of nanoparticles. SA led to the lowest extent of hemolysis possibly because of its lowest surface charge whereas amine-modified mesoporous SiO<sub>2</sub> caused similar rates of hemolysis. The concentrations of SiO<sub>2</sub> leading to 10% hemolysis (LC<sub>10</sub>) are summarized in Table 5. Zhao et al<sup>37</sup> revealed that the affinity of SiO<sub>2</sub> to RBCs decreased with increasing degree of surface functionality independent of surface charge (–43 mV – 7 mV). Results from our study as shown in Table 5 suggest that increasing the surface charge beyond a certain threshold (> 30 mV) might lead to an opposite effect including enhanced interaction of nanoparticles with RBCs and the resultant elevated hemolysis by amine-modified mesoporous SiO<sub>2</sub>, in agreement with the cellular association results (Figure 6A–B). It must be noted that a good correlation with results of different experiments is based on a similar dose (ca. ≤ 100 µg/mL SiO<sub>2</sub>). As the dose changes beyond a certain range, the pattern from

different experiments would shift and the correlation of various experiments at that dosage need to be further validated.

## CONCLUSION

In summary, nonporous Stöber silica nanospheres, mesoporous silica nanospheres, mesoporous silica nanorods with aspect ratio of 2, 4 and 8, as well as their cationic charged counterparts were synthesized and characterized. The porosity, shape and surface modification effects on cellular toxicity or hemolytic activity were evaluated on macrophages, cancer epithelial cells, or on human erythrocytes. The toxicity of SiO<sub>2</sub> was found to be cell-type dependent. Cancer epithelial cells were highly resistant to nanoparticle treatment while the toxicity on macrophages was predominantly surface charge-dependent. The difference in toxicity between the two cell types could be due to the difference in the physiological function of each. Porosity and surface characteristics of the nanoparticles were the major factors that influenced the cellular association of the nanoparticles. Geometry did not seem to influence the extent of cellular association of the nanoparticles at either the early time point or over extended duration. Initial comparison of blood biocompatibility of nonporous and mesoporous SiO<sub>2</sub> with varied shapes and surface characteristics has been demonstrated using the hemolysis assay. Bare SiO<sub>2</sub> showed a porosity- and geometry-dependent hemolytic activity on RBCs with mesoporous SiO<sub>2</sub> at high aspect ratio exhibiting a reduced hemolytic activity. The extent of hemolysis was highly zeta potential-dependent among the amine-modified SiO<sub>2</sub> and results indicated that there could be a surface charge “threshold” below which the amine modification on SiO<sub>2</sub> could lead to reduced hemolysis compared with their bare counterparts. Further studies evaluating the *in vivo* toxicity of SiO<sub>2</sub> in animal models are needed to establish an *in vitro-in vivo* correlation for better prediction of toxicity in biological systems.

## METHODS

### Synthesis of Nonporous and Mesoporous SiO<sub>2</sub>

Nonporous silica nanoparticles (Stöber) were produced using the modified Stöber method.<sup>23</sup> 34.82 mL water, 3.25 mL ammonium hydroxide (29.7%), and 100 mL ethanol were mixed and stabilized at 40 °C. 6.20 mL tetraethyl orthosilicate (TEOS) was added at an injection rate of 5 mL/min upon stirring at 550 rpm. The reaction was conducted for 1 hour and the product was washed twice by ethanol and stored in ethanol. Mesoporous SiO<sub>2</sub> of different shapes was synthesized through a one-step condensation under dilute silica source and low surfactant concentration conditions with ammonium hydroxide as the base catalyst.<sup>24–29</sup> Generally, cetyltrimethylammonium bromide (CTAB) was dissolved in aqueous medium with mild heating (30 °C). After the solution was cooled to room temperature (22 °C), aqueous ammonia was introduced and the mixture was stirred for an hour. TEOS was added at the rate of 5 mL/minute while the stirring continued. The mixture was further stirred for 4 hours and the product was autoclaved at 100 °C for 24 hours.<sup>30, 31</sup> Subsequently the product was collected by centrifugation at 15,000 rpm for 20 minutes. As-synthesized nanoparticles were suspended in ethanolic HCl (1.5 mL HCl in 150 mL ethanol) and heated at 60°C for 6 hours to remove the surfactant. The complete removal of CTAB was confirmed by Fourier transform infrared (FT-IR) spectroscopy.

### Surface Functionalization

To modify the surface of SiO<sub>2</sub> with primary amine functionalities,<sup>33</sup> 100 mg of SiO<sub>2</sub> were resuspended in 100 mL of anhydrous ethanol. (3-aminopropyl)triethoxysilane (APTES) was introduced drip by drip to SiO<sub>2</sub> suspension upon stirring at 500 rpm under nitrogen flow. The mixture was stirred at room temperature for 20 hours. Amine-modified SiO<sub>2</sub> were



collected by centrifugation and washed extensively with ethanol and water. SiO<sub>2</sub> were stored in ethanol at 4°C and transferred to water immediately before use.

### Nanoparticle Characterization

Transmission electron microscopy (TEM) images were taken with a Philips Tecnai microscope operating at 120 kV. FT-IR spectra were recorded on a Varian Cary FTIR 1000 spectrometer using KBr pellets. X-ray diffraction (XRD) patterns of SiO<sub>2</sub> were analyzed on a Philips PANalytical X'Pert X-ray diffractometer (Spectris, England) using Cu K $\alpha$  radiation ( $\lambda = 0.1542$  nm) at 45 kV and 40 mA. The XRD spectra were recorded in the  $2\theta$  range of 2–10 with a step size of 0.02° in a  $2\theta$  scattering angle and a scanning speed of 0.01 degree/second. The slit sizes and specimen length were also adjusted for divergence slit, anti-scattered slit, and receiving slit to suit for the low angle detection. Nitrogen adsorption–desorption isotherm measurements were completed on a Micromeritics ASAP 2010 (Norcross, GA) accelerated surface area analyzer at –196 °C. The SiO<sub>2</sub> were dried at 100 °C for overnight before analysis. The Brunauer–Emmett–Teller (BET) specific surface areas were calculated by using adsorption data at  $P/P_0 = 0.05–0.20$ .<sup>19, 21</sup> The external surface areas of mesoporous SiO<sub>2</sub> were calculated from the  $t$  plots of their N<sub>2</sub> adsorption isotherms.<sup>32</sup> Pore volume and Pore size distributions were obtained from adsorption branch by using the Barrett, Joyner, and Halenda (BJH) method.<sup>19, 21</sup>

### Acute Cytotoxicity Assay

The acute toxicity effect of SiO<sub>2</sub> was determined by WST-8 assay on A549 cells or RAW 264.7 (ATCC, Manassas, VA). Cells from passages 5 through 20 were used with medium changing once every three days. A549 cells or RAW 264.7 macrophages were seeded at 8,000 cells/well or 16,000 cells/well in a 96-well plate in F-12k medium or DMEM supplemented with 10% FBS and maintained in a humidified incubator for 24 hours. SiO<sub>2</sub> at incremental concentration of 100, 250, or 500  $\mu\text{g}/\text{mL}$  were added to cells. Supernatants from nanoparticle stock solutions and respective growth medium only were served as controls. Post 24 hours, old medium was aspirated and cells were washed three times with PBS. 100  $\mu\text{L}$  complete medium containing 10% (v/v) Cell Counting Kit-8 (Dojindo, Rockville, MD) was added to each well and incubated with cells for two hours. The absorbance of the plate was recorded at 450 nm on a UV/Vis reader with a reference wavelength of 650 nm.

### Proliferation Inhibition Assay

The cytotoxicity of SiO<sub>2</sub> was evaluated by WST-8 viability assay on A549 cells or RAW264.7 macrophages. Initially, A549 or RAW cells were seeded at 2,000 cells/well or 4,000 cells/well in a 96-well plate and allowed settlement for 24 hours. 10, 50, 100, 250, 500, or 1,000  $\mu\text{g}/\text{mL}$  of bare SiO<sub>2</sub> or amine-modified SiO<sub>2</sub> were added into the 96-well plate in triplicates. Supernatants from nanoparticle stock solutions and respective growth medium only were served as controls. Post 72 hours, old medium was aspirated and the following steps were the same as the procedures for acute cytotoxicity assay described above.

### Plasma Membrane Integrity Assay

Determination of propidium iodide uptake was used to assess the integrity of plasma membrane of nanoparticle-dosed cells. A549 cells or RAW cells were seeded at  $8 \times 10^4$  cells/well or  $1.6 \times 10^5$  cells/well on a 12-well plate in triplicate. After 24 hours, selected nanoparticles were added into each well at the concentration of 250  $\mu\text{g}/\text{mL}$ . 24 hours later, cells and medium from each well were collected into a 5 mL flow cytometry tube. The cell suspension was centrifuged at 1000 rpm  $\times$  5 minutes, supernatant was decanted, and the cells were resuspended in 100  $\mu\text{L}$  of PBS. 5  $\mu\text{L}$  of propidium iodide solution (50  $\mu\text{g}/\text{mL}$  in water) was added to each tube. The tube was gently vortexed and incubated for 15 minutes

at room temperature in the dark. 400  $\mu\text{L}$  of PBS was added into each tube and the samples were analyzed by flow cytometry (FACScan Analyzer, Becton Dickinson, Franklin Lakes, NJ) within an hour.

### Quantitation of Cellular Association

Cellular association of  $\text{SiO}_2$  was evaluated on A549 cells and RAW264.7 cells. A549 cells or RAW cells were seeded at  $8 \times 10^4$  cells/well or  $1.6 \times 10^5$  cells/well on a 12-well plate in triplicate, 24 hours before the addition of particles. Cells were incubated with 100  $\mu\text{g}/\text{mL}$  of  $\text{SiO}_2$  for 24 hours ( $37^\circ\text{C}$ , 5%  $\text{CO}_2$ ). After cell/particle incubation, the old medium was aspirated and the cells were washed three times with PBS. Then the cells were treated with 0.5 mL of 0.1% (v/v) Triton X-100 solution in water for 15 minutes. After that, the cell lysate was collected into a centrifuge tube and the wells were further washed with 0.5 mL water. The wash was also collected into the same centrifuge tube. 100  $\mu\text{L}$  aliquots of cell lysate were used for protein content measurement by BCA assay (Thermo Scientific, Rockford, IL). The concentration of silicon in the cell lysate was measured by direct Si measurement using inductively coupled plasma mass spectrometry (ICP-MS, Agilent 7500, Agilent Technologies, Santa Clara, CA). The amount of cellular associated  $\text{SiO}_2$  post 1 hour incubation at  $4^\circ\text{C}$  or  $37^\circ\text{C}$  was also measured. RAW cells were seeded at  $3.2 \times 10^5$  cells/well on a 12-well plate in triplicate and incubated for 24 hours. After that, cells were preconditioned to  $4^\circ\text{C}$  by incubating at  $4^\circ\text{C}$  for a brief period of 10 minutes. Then silica nanoparticles were added to the cells at the concentration of 100  $\mu\text{g}/\text{mL}$  and the cells were further incubated at  $4^\circ\text{C}$  for another hour. Following treatment was the same as mentioned above. To make sure that relative cell viability in the  $4^\circ\text{C}$  treated plate was not dramatically influenced by exposure to cold temperature for the experimental duration, the relative viability from  $4^\circ\text{C}$  treated plate was compared with cells incubated at  $37^\circ\text{C}$  for 70 minutes by WST-8 assay.

### Hemolysis

Heparin-stabilized human blood was freshly collected according to an approved University of Utah Institutional Review Board protocol and used within 3 hours of being drawn.<sup>36, 43</sup> 4 mL of whole blood was added to 8 mL of Dulbecco's phosphate buffered saline (D-PBS) and the RBCs were isolated from serum by centrifugation at  $10,016 \times g$  for 5 minutes. The RBCs were further washed five times with sterile D-PBS solution. Following the last wash, the RBCs were diluted to 40 mL of D-PBS. 0.2 mL of the diluted RBC suspension was added to 0.8 mL of silica nanoparticle suspension in D-PBS at the concentration of 12.5  $\mu\text{g}/\text{mL}$ , 62.5  $\mu\text{g}/\text{mL}$ , 125  $\mu\text{g}/\text{mL}$ , 312.5  $\mu\text{g}/\text{mL}$  or 625  $\mu\text{g}/\text{mL}$  to make the final nanoparticle concentration at 10, 50, 100, 250, or 500  $\mu\text{g}/\text{mL}$ . All samples were prepared in triplicate and the suspension was briefly vortexed before leaving at static condition at room temperature for 4 hours. After that, the mixture was briefly vortexed again and centrifuged at  $10,016 \times g$  for 3 minutes. 100  $\mu\text{L}$  of supernatant from the sample tube was transferred to a 96-well plate. The absorbance value of hemoglobin at 577 nm was measured with the reference wavelength at 655 nm. 0.2 mL diluted RBC suspensions incubated with 0.8 mL of D-PBS and 0.8 mL of water were used as the negative or positive control. The percent of hemolysis was calculated as:

$$\text{Hemolysis \%} = [(\text{Sample absorbance} - \text{negative control}) / (\text{positive control} - \text{negative control})] \times 100\%$$

### Statistical Analysis

The difference between multiple groups was analyzed by one-way ANOVA, Tukey post test was used where difference was detected. For two group comparison Student's *t*-test was

used. The difference between two groups was considered significant when  $p < 0.05$ . The  $LC_{10}$  values in hemolysis assay were determined by using ED50plus v1.0 software.

## Supplementary Material

Refer to Web version on PubMed Central for supplementary material.

## Acknowledgments

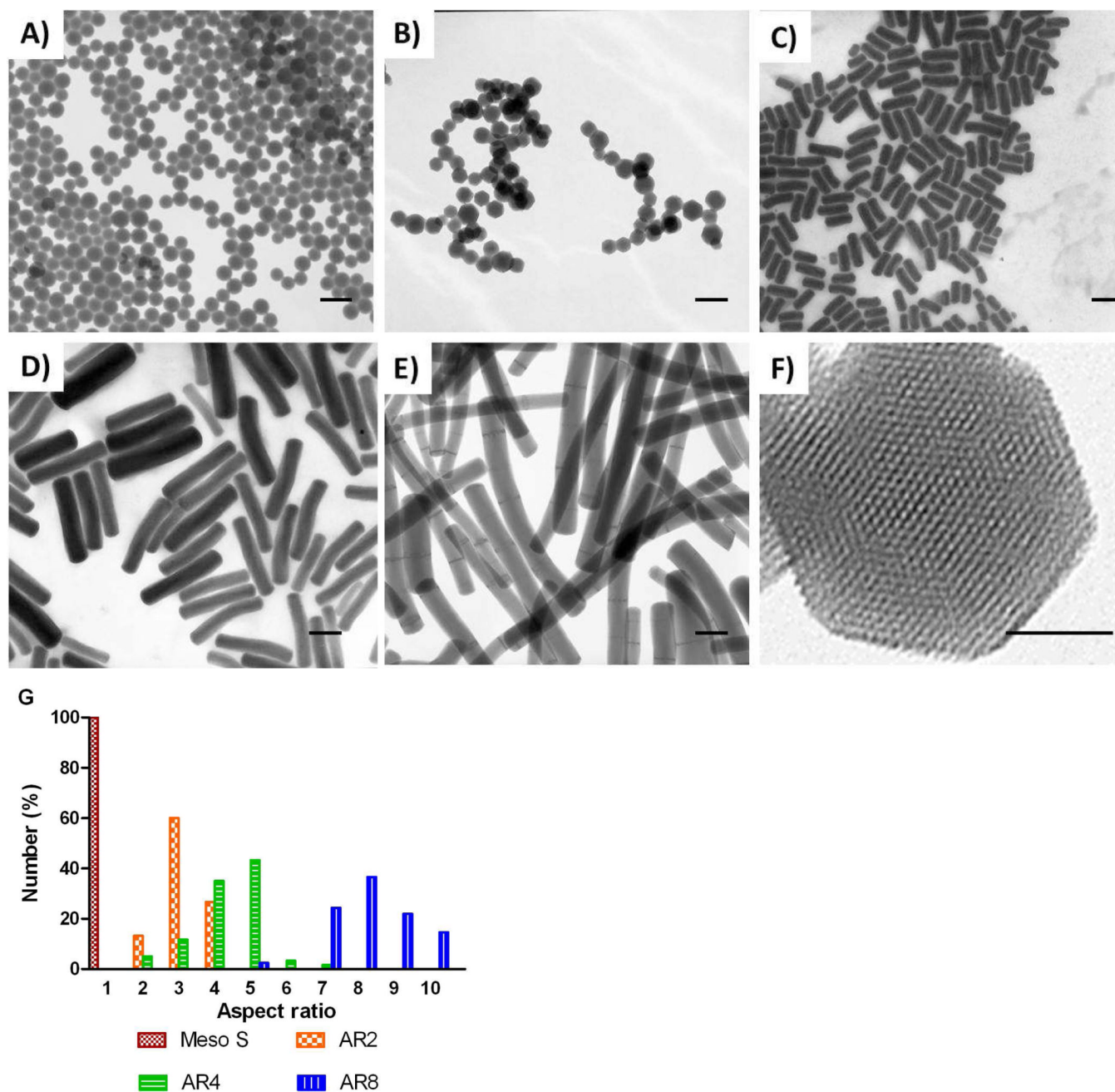
We would like to acknowledge Dr. Sajo Naik (Western Research Institute, Cheyenne, WY) for his technical suggestions for mesoporous silica nanoparticle synthesis, and Dr. Khaled Greish for assistance with human blood withdrawal from lab volunteers. Financial support was provided by NIH grant (R01 DE19050) and the Utah Science and Technology Research (USTAR) Initiative.

## REFERENCES AND NOTES

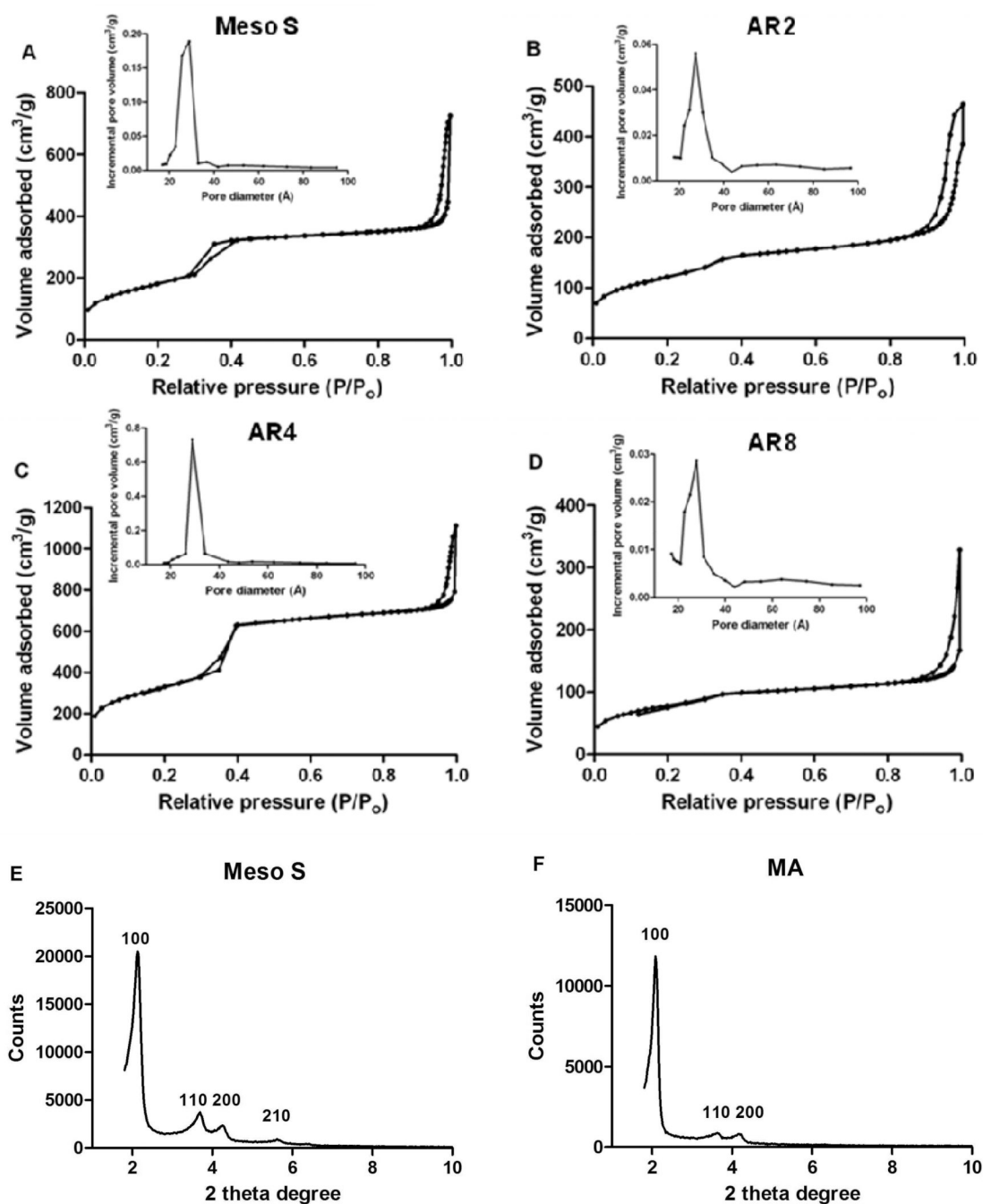
1. Barbé C, Bartlett J, Kong L, Finnie K, Lin H, Larkin M, Calleja S, Bush A, Calleja G. Silica Particles: A Novel Drug-Delivery System. *Adv. Mater.* 2004; 16:1–8.
2. Liong M, Lu J, Kovichich M, Xia T, Ruehm SG, Nel AE, Tamanoi F, Zink JI. Multifunctional Inorganic Nanoparticles for Imaging, Targeting, and Drug Delivery. *ACS Nano.* 2008; 2:889–896. [PubMed: 19206485]
3. Vivero-Escoto JL, Slowing II, Trewyn BG, Lin VS. Mesoporous Silica Nanoparticles for Intracellular Controlled Drug Delivery. *Small.* 2010; 6:1952–1967. [PubMed: 20690133]
4. Lu J, Liong M, Li Z, Zink JI, Tamanoi F. Biocompatibility, Biodistribution, and Drug-Delivery Efficiency of Mesoporous Silica Nanoparticles for Cancer Therapy in Animals. *Small.* 2010; 6:1794–1805. [PubMed: 20623530]
5. Li L, Tang F, Liu H, Liu T, Hao N, Chen D, Teng X, He J. *In Vivo* Delivery of Silica Nanorattle Encapsulated Docetaxel for Liver Cancer Therapy with Low Toxicity and High Efficacy. *ACS Nano.* 2010; 4:6874–6882. [PubMed: 20973487]
6. Tsai C-P, Chen C-Y, Hung Y, Chang F-H, Mou C-Y. Monoclonal Antibody-Functionalized Mesoporous Silica Nanoparticles (MSN) for Selective Targeting Breast Cancer Cells. *J. Mater. Chem.* 2009; 19:5737–5743.
7. Cheng S-H, Lee C-H, Chen M-C, Souris JS, Tseng F-G, Yang C-S, Mou C-Y, Chen C-T, Lo L-W. Tri-Functionalization of Mesoporous Silica Nanoparticles for Comprehensive Cancer Theranostics—the Trio of Imaging, Targeting and Therapy. *J. Mater. Chem.* 2010; 20:6149–6157.
8. Nan A, Bai X, Son SJ, Lee SB, Ghandehari H. Cellular Uptake and Cytotoxicity of Silica Nanotubes. *Nano Lett.* 2008; 8:2150–2154. [PubMed: 18624386]
9. Son SJ, Bai X, Nan A, Ghandehari H, Lee SB. Template Synthesis of Multifunctional Nanotubes for Controlled Release. *J Control Release.* 2006; 114:143–152. [PubMed: 16870299]
10. Chen C-C, Liu Y-C, Wu C-H, Yeh C-C, Su M-T, Wu Y-C. Preparation of Fluorescent Silica Nanotubes and Their Application in Gene Delivery. *Adv. Mater.* 2005; 17:404–407.
11. Buyukserin F, Medley CD, Mota MO, Kececi K, Rogers RR, Tan W, Martin CR. Antibody-Functionalized Nano Test Tubes Target Breast Cancer Cells. *Nanomedicine (Lond).* 2008; 3:283–292. [PubMed: 18510424]
12. Hudson SP, Padera RF, Langer R, Kohane DS. The Biocompatibility of Mesoporous Silicates. *Biomaterials.* 2008; 29:4045–4055. [PubMed: 18675454]
13. Gratton SE, Ropp PA, Pohlhaus PD, Luft JC, Madden VJ, Napier ME, DeSimone JM. The Effect of Particle Design on Cellular Internalization Pathways. *Proc Natl Acad Sci U S A.* 2008; 105:11613–11618. [PubMed: 18697944]
14. Muro S, Garnacho C, Champion JA, Leferovich J, Gajewski C, Schuchman EH, Mitragotri S, Muzykantov VR. Control of Endothelial Targeting and Intracellular Delivery of Therapeutic Enzymes by Modulating the Size and Shape of ICAM-1-Targeted Carriers. *Mol Ther.* 2008; 16:1450–1458. [PubMed: 18560419]

15. Arnida, Janat-Amsbury MM, Ray A, Peterson CM, Ghandehari H. Geometry and Surface Characteristics of Gold Nanoparticles Influence Their Biodistribution and Uptake by Macrophages. *Eur J Pharm Biopharm.* 2011; 77:417–423. [PubMed: 21093587]
16. Nguyen TPB, Lee J-W, Shim WG, Moon H. Synthesis of Functionalized SBA-15 with Ordered Large Pore Size and Its Adsorption Properties of BSA. *Microporous and Mesoporous Materials.* 2008; 110:560–569.
17. Maurer-Jones MA, Lin YS, Haynes CL. Functional Assessment of Metal Oxide Nanoparticle Toxicity in Immune Cells. *ACS Nano.* 2010; 4:3363–3373. [PubMed: 20481555]
18. Slowing I, Trewyn BG, Lin VS. Effect of Surface Functionalization of MCM-41-Type Mesoporous Silica Nanoparticles on the Endocytosis by Human Cancer Cells. *J Am Chem Soc.* 2006; 128:14792–14793. [PubMed: 17105274]
19. Lu F, Wu SH, Hung Y, Mou CY. Size Effect on Cell Uptake in Well-Suspended, Uniform Mesoporous Silica Nanoparticles. *Small.* 2009; 5:1408–1413. [PubMed: 19296554]
20. He Q, Zhang Z, Gao Y, Shi J, Li Y. Intracellular Localization and Cytotoxicity of Spherical Mesoporous Silica Nano- and Microparticles. *Small.* 2009; 5:2722–2729. [PubMed: 19780070]
21. Tsai CP, Hung Y, Chou YH, Huang DM, Hsiao JK, Chang C, Chen YC, Mou CY. High-Contrast Paramagnetic Fluorescent Mesoporous Silica Nanorods as a Multifunctional Cell-Imaging Probe. *Small.* 2008; 4:186–191. [PubMed: 18205156]
22. Dobrovolskaia MA, Aggarwal P, Hall JB, McNeil SE. Preclinical Studies to Understand Nanoparticle Interaction with the Immune System and Its Potential Effects on Nanoparticle Biodistribution. *Mol Pharm.* 2008; 5:487–495. [PubMed: 18510338]
23. Chung YS, Jeon MY, Kim CK. Fabrication of Nearly Monodispersed Silica Nanoparticles by Using Poly(1-Vinyl-2-Pyrrolidinone) and Their Application to the Preparation of Nanocomposites. *Macromol. Res.* 2009; 17:37–43.
24. Giri S, Trewyn BG, Stellmaker MP, Lin VS-Y. Stimuli-Responsive Controlled-Release Delivery System Based on Mesoporous Silica Nanorods Capped with Magnetic Nanoparticles. *Angew. Chem. Int. Ed.* 2005; 44:5038–5044.
25. Huh S, Wiench JW, Yoo J-C, Pruski M, Lin VS-Y. Organic Functionalization and Morphology Control of Mesoporous Silicas Via a Co-Condensation Synthesis Method. *Chem. Mater.* 2003; 15:4247–4256.
26. Naik SP, Elangovan SP, Okubo T, Sokolov I. Morphology Control of Mesoporous Silica Particles. *J. Phys. Chem. C.* 2007; 111:11168–11173.
27. Yang S, Zhao L, Yu C, Zhou X, Tang J, Yuan P, Chen D, Zhao D. On the Origin of Helical Mesostuctures. *J Am Chem Soc.* 2006; 128:10460–10466. [PubMed: 16895411]
28. Lelong G, Bhattacharyya S, Kline S, Cacciaguerra T, Gonzalez MA, Saboungi M-L. Effect of Surfactant Concentration on the Morphology and Texture of MCM-41 Materials. *J. Phys. Chem. C.* 2008; 112:10674–10680.
29. Jin H, Liu Z, Ohsuna T, Terasaki O, Inoue Y, Sakamoto K, Nakanishi T, Ariga K, Che S. Control of Morphology and Helicity of Chiral Mesoporous Silica. *Adv. Mater.* 2006; 18:593–596.
30. Kim JM, Kwak JH, Jun S, Ryoo R. Ion Exchange and Thermal Stability of MCM-41. *J. Phys. Chem.* 1995; 99:16742–16747.
31. Ryoo R, Jun S. Improvement of Hydrothermal Stability of MCM-41 Using Salt Effects During the Crystallization Process. *J. Phys. Chem. B.* 1997; 101:317–320.
32. Zhu HY, Zhao XS, Liu GQ, Do DD. Improved Comparison Plot Method for Pore Structure Characterization of MCM-41. *Langmuir.* 1996; 12:6513–6517.
33. Kobler J, Moller K, Bein T. Colloidal Suspensions of Functionalized Mesoporous Silica Nanoparticles. *ACS Nano.* 2008; 2:791–799. [PubMed: 19206612]
34. Jones CF, Grainger DW. *In Vitro* Assessments of Nanomaterial Toxicity. *Adv Drug Deliv Rev.* 2009; 61:438–456. [PubMed: 19383522]
35. Riccardi C, Nicoletti I. Analysis of Apoptosis by Propidium Iodide Staining and Flow Cytometry. *Nat Protoc.* 2006; 1:1458–1461. [PubMed: 17406435]
36. Slowing II, Wu CW, Vivero-Escoto JL, Lin VS. Mesoporous Silica Nanoparticles for Reducing Hemolytic Activity Towards Mammalian Red Blood Cells. *Small.* 2009; 5:57–62. [PubMed: 19051185]

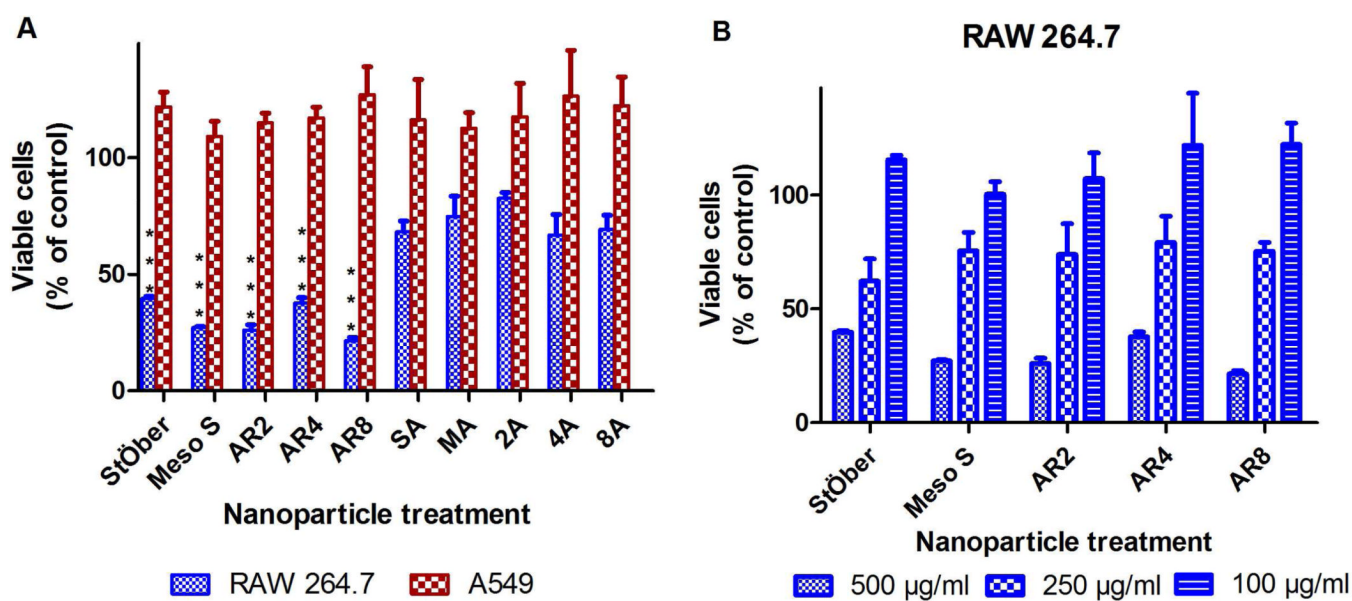
37. Zhao Y, Sun X, Zhang G, Trewyn BG, Slowing II, Lin VS. Interaction of Mesoporous Silica Nanoparticles with Human Red Blood Cell Membranes: Size and Surface Effects. *ACS Nano*. 2011; 5:1366–1375. [PubMed: 21294526]
38. Xing X, He X, Peng J, Wang K, Tan W. Uptake of Silica-Coated Nanoparticles by HeLa Cells. *J Nanosci Nanotechnol*. 2005; 5:1688–1693. [PubMed: 16245529]
39. Tao Z, Toms BB, Goodisman J, Asefa T. Mesoporosity and Functional Group Dependent Endocytosis and Cytotoxicity of Silica Nanomaterials. *Chem Res Toxicol*. 2009; 22:1869–1880. [PubMed: 19817448]
40. Petushkov A, Intra J, Graham JB, Larsen SC, Salem AK. Effect of Crystal Size and Surface Functionalization on the Cytotoxicity of Silicalite-1 Nanoparticles. *Chem Res Toxicol*. 2009; 22:1359–1368. [PubMed: 19580308]
41. Chung TH, Wu SH, Yao M, Lu CW, Lin YS, Hung Y, Mou CY, Chen YC, Huang DM. The Effect of Surface Charge on the Uptake and Biological Function of Mesoporous Silica Nanoparticles in 3T3-L1 Cells and Human Mesenchymal Stem Cells. *Biomaterials*. 2007; 28:2959–2966. [PubMed: 17397919]
42. Nabeshi H, Yoshikawa T, Arimori A, Yoshida T, Tochigi S, Hirai T, Akase T, Nagano K, Abe Y, Kamada H, et al. Effect of Surface Properties of Silica Nanoparticles on Their Cytotoxicity and Cellular Distribution in Murine Macrophages. *Nanoscale Research Letters*. 2011; 6:1–6.
43. Lin YS, Haynes CL. Impacts of Mesoporous Silica Nanoparticle Size, Pore Ordering, and Pore Integrity on Hemolytic Activity. *J Am Chem Soc*. 2010; 132:4834–4842. [PubMed: 20230032]
44. Jan KM, Chien S. Role of Surface Electric Charge in Red Blood Cell Interactions. *J Gen Physiol*. 1973; 61:638–654. [PubMed: 4705641]



**Figure 1.** Transmission electron microscopy images of A) Stöber SiO<sub>2</sub> with average diameter of 115 nm (referred to as Stöber), B) mesoporous SiO<sub>2</sub> with average diameter of 120 nm (Meso S), C) mesoporous silica nanorods with aspect ratio 2 (AR2), D) mesoporous silica nanorods with aspect ratio 4 (AR4), E) mesoporous silica nanorods with aspect ratio 8 (AR8), and F) high resolution image of a single particle in B), G) The percentage distribution histogram as a function of aspect ratio. Scale bars in A–E = 200 nm, scale bar in F = 50 nm.

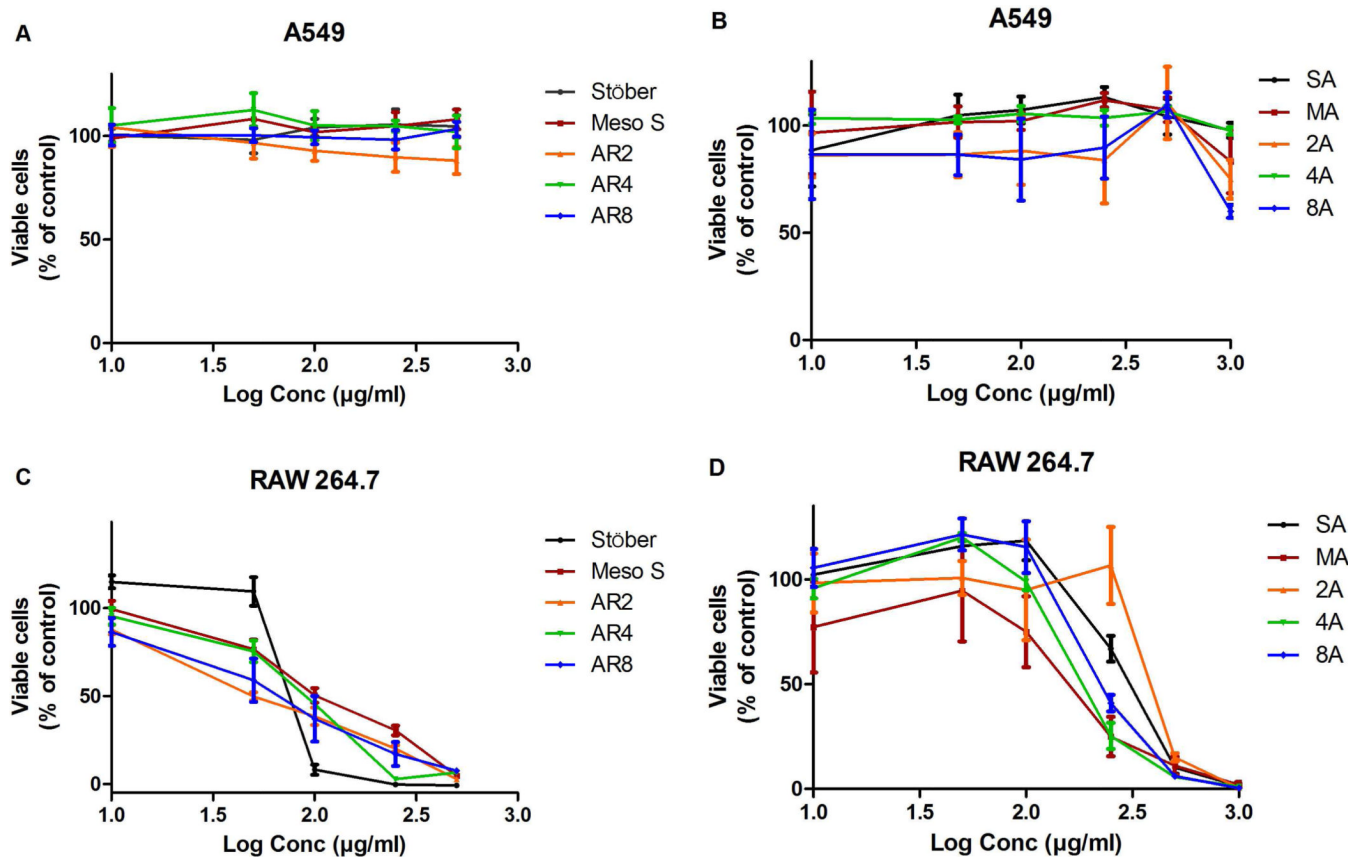


**Figure 2.** Nitrogen adsorption-desorption isotherms of: A) Meso S, B) AR2, C) AR4, D) AR8 mesoporous SiO<sub>2</sub>. Inserts are pore size distribution plots for each type of SiO<sub>2</sub>. X-ray diffraction patterns of: E) Meso S, and F) MA. Both Meso S and MA exhibited the typical diffraction patterns of MCM-41 type mesoporous SiO<sub>2</sub> with hexagonal symmetry. The reduction in intensity of MA diffraction pattern and the missing 210 peak might be due to the pore filling effects caused by silane modification.<sup>21</sup>

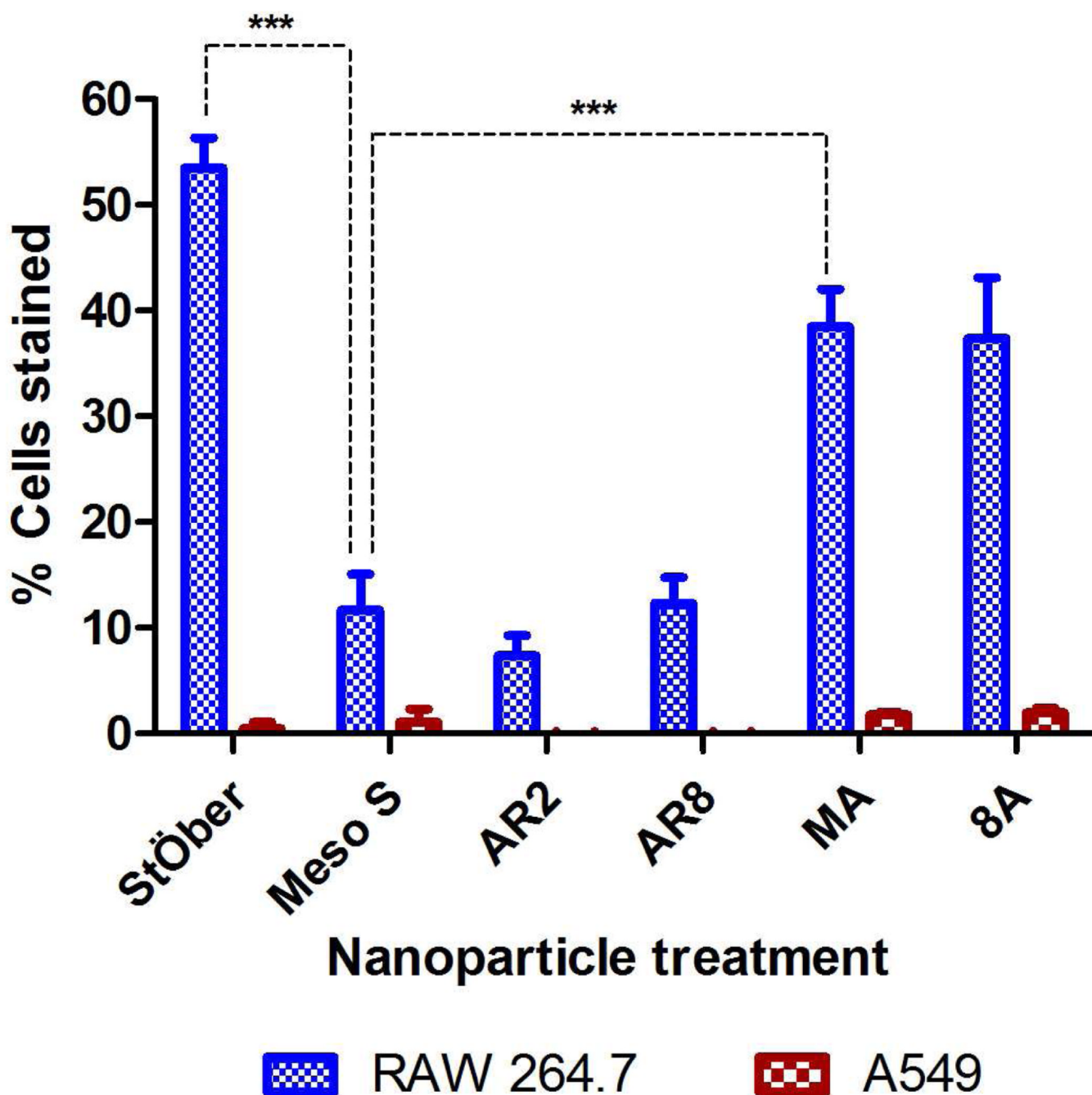
**Figure 3.**

Acute cytotoxicity assay of indicated cells incubated with: A) bare and amine-modified  $\text{SiO}_2$  at 500  $\mu\text{g/mL}$ , B) Acute cytotoxicity assay of RAW 264.7 cells after incubating with bare  $\text{SiO}_2$  at 500  $\mu\text{g/mL}$ , 250  $\mu\text{g/mL}$  and 100  $\mu\text{g/mL}$  for 24 hours. \*\*\* Relative viability of bare silica nanoparticle-treated cells was significantly lower than that of amine-modified counterpart-treated cells ( $p < 0.001$ ). Data were mean  $\pm$  SD ( $n = 3$ ).

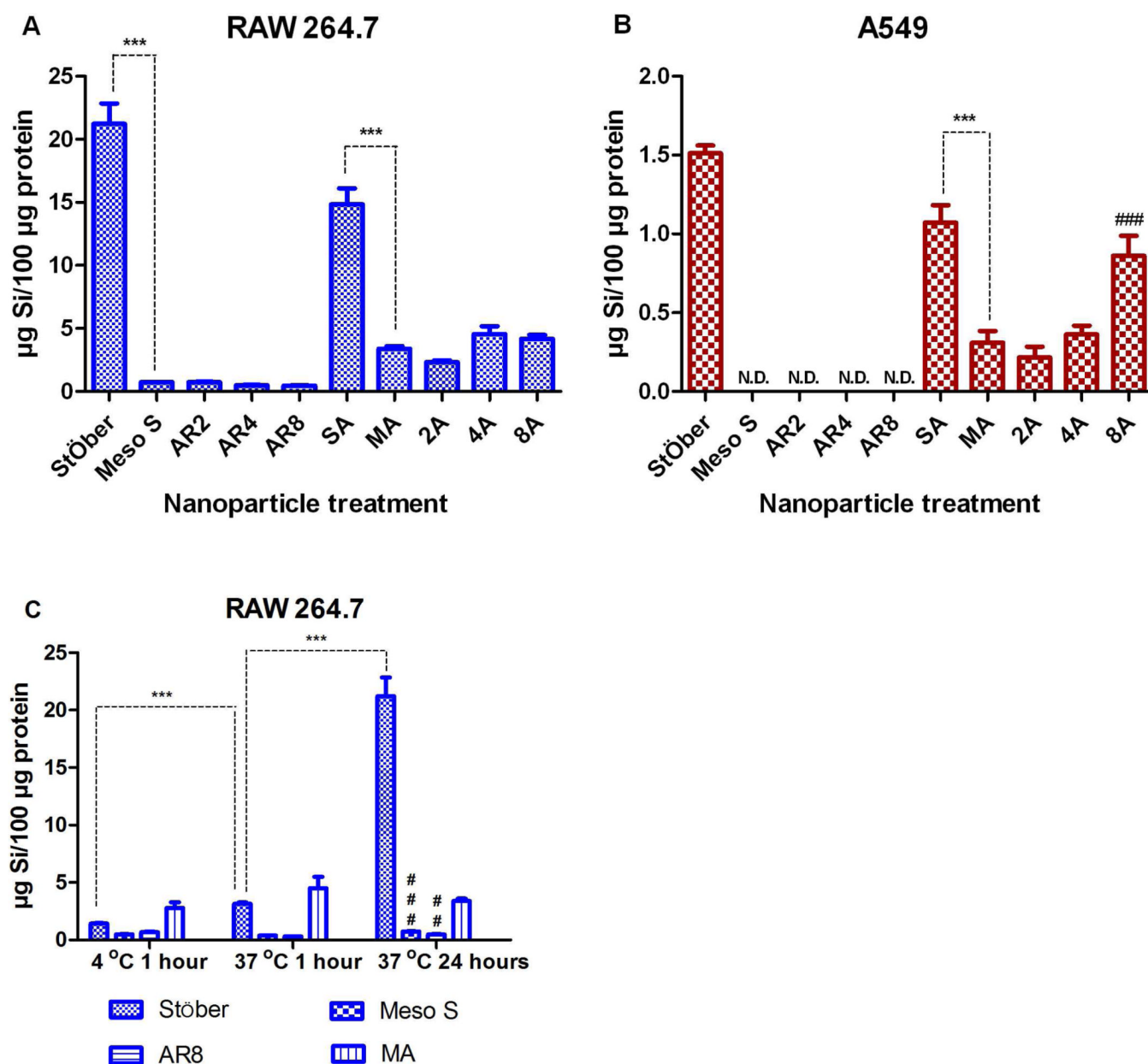




**Figure 4.** Proliferation inhibition assay of A549 (A, B) and RAW 264.7 (C, D) cells after continuous 72 hours incubation with bare (A, C) and amine-modified (B, D) SiO<sub>2</sub>. Data were mean ± SD (n = 3).



**Figure 5.** Percentage of propidium iodide stained cells in RAW 264.7 cells (blue bars) or A549 cells (red bars) after incubating with 250  $\mu\text{g/mL}$   $\text{SiO}_2$  for 24 hours. \*\*\*Meso S led to significantly decreased percentage of propidium iodide-positive cells compared with Stöber or MA ( $p < 0.001$ ). Data were mean  $\pm$  SD ( $n = 3$ ).

**Figure 6.**

Inductively coupled plasma mass spectrometry (ICP-MS) analysis of cellular association of SiO<sub>2</sub> in: A) RAW 264.7 and B) A549 cells post incubation with nanoparticles at 100 µg/mL for 24 hours. The graph shows the mass of silicon per 100 µg protein content versus different nanoparticle treatments. \*\*\*The level of cell-associated silicon was significantly higher in Stöber or SA treated cells than in the mesoporous counterpart treated cells ( $p < 0.001$ ). ### The level of cell-associated silicon was significantly higher in high aspect ratio, 8A treated cells than in MA, 2A or 4A treated cells ( $p < 0.001$ ). N.D. means “not detected”. C) Cellular association of SiO<sub>2</sub> after RAW 264.7 cells were incubated with 100 µg/mL selected SiO<sub>2</sub> at 4 °C (1 hour) and 37 °C (1 hour or 24 hours). The level of cellular associated silicon was significantly higher at 24 hours than at 1 hour post incubation with Stöber (\*\*\*,  $p < 0.001$ ), Meso S (###,  $p < 0.001$ ) or AR8 (##,  $p < 0.01$ ) at 37 °C. 1 hour

incubation with Stöber at 37 °C led to significantly higher silicon association than incubation at 4 °C (\*\*\*,  $p < 0.001$ ). Data were mean  $\pm$  SD ( $n = 3$ ).

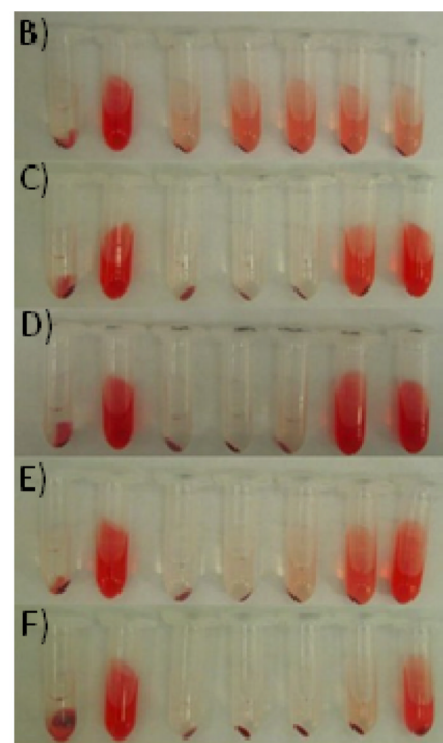
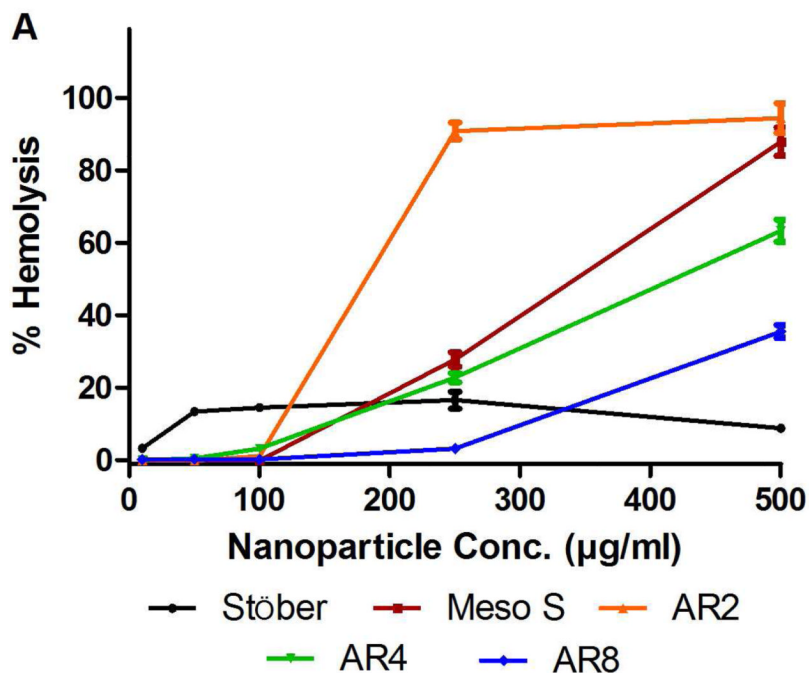


**Figure 7.**

Hemolysis assay on bare SiO<sub>2</sub>: A) Relative rate of hemolysis in human RBCs upon incubation with nanoparticle suspension at incremental concentrations. The presence of hemoglobin in the supernatant (red) was observed in: B) Stöber suspension, C) Meso S suspension, D) AR2 suspension, E) AR4 suspension, and F) AR8 suspension. The tubes were lined in a sequence (from left to right) as negative control (PBS), positive control (water), 10 µg/mL suspension, 50 µg/mL suspension, 100 µg/mL suspension, 250 µg/mL suspension, and 500 µg/mL suspension. Data were mean ± SD (n = 3).

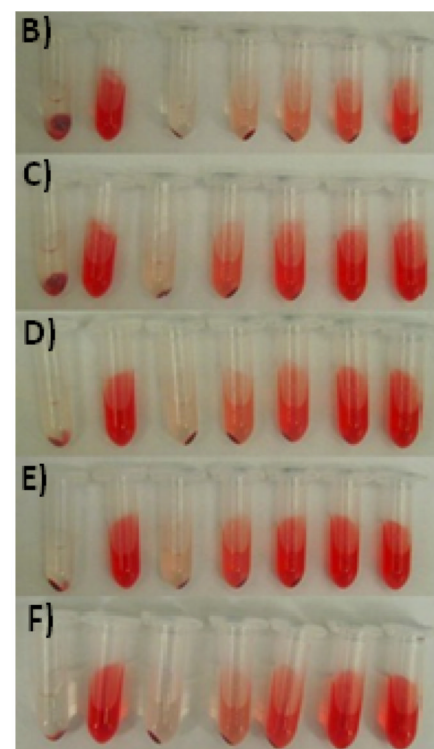
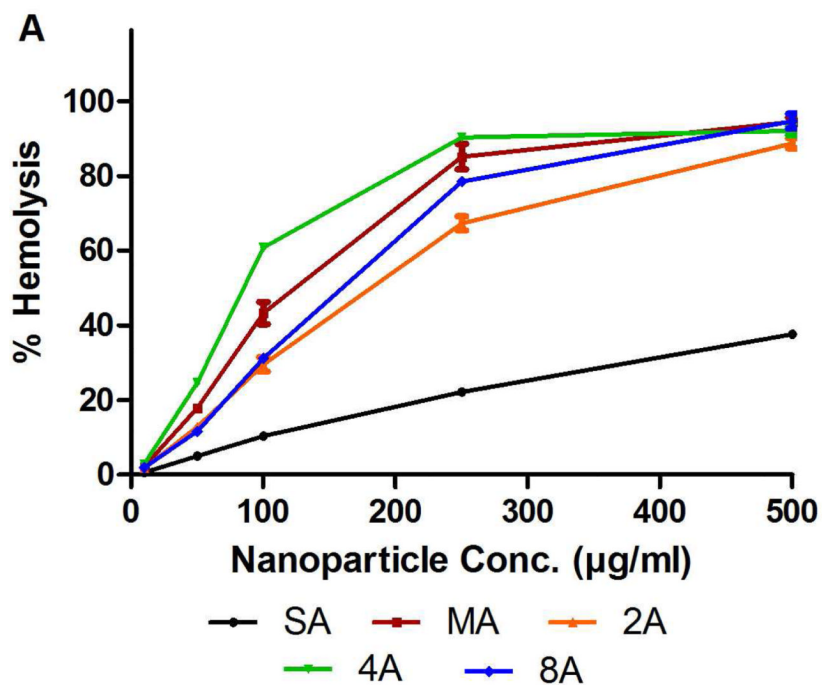


**Figure 8.** Hemolysis assay on amine-modified SiO<sub>2</sub>: A) Relative rate of hemolysis in human RBCs upon incubation with amine-modified nanoparticle suspension at incremental concentrations. The presence of hemoglobin in the supernatant (red) was observed in: B) SA suspension, C) MA suspension, D) 2A suspension, E) 4A suspension, and F) 8A suspension. The tubes were lined in a sequence (from left to right) as negative control (PBS), positive control (water), 10 µg/mL suspension, 50 µg/mL suspension, 100 µg/mL suspension, 250 µg/mL suspension, and 500 µg/mL suspension. Data were mean ± SD (n = 3).

Synthetic conditions of nonporous and mesoporous  $\text{SiO}_2$  and their physical characterization of size, surface area and pore size.\*

**Table 1**

|               | Composition<br>(CTAB:H <sub>2</sub> O:<br>NH <sub>4</sub> OH:TEOS) | Stirring<br>rate<br>(RPM) | Temp.<br>(°C) | Size by TEM (nm)      | Aspect<br>ratio | Surface<br>area<br>(m <sup>2</sup> /g) | External<br>surface<br>area (m <sup>2</sup> /g) | Pore<br>volume<br>(cm <sup>3</sup> /g) | Pore<br>size<br>(nm) |
|---------------|--|---------------------------|---------------|-----------------------|-----------------|--|---|--|----------------------|
| <b>Stöber</b> | See "METHODS"  | 550                       | 40            | 115 ± 13              | 1.0             | 24 <sup>#</sup>                        | 24 <sup>#</sup>                                 | N/A                                    | N/A                  |
| <b>Meso S</b> | 0.1:1000:7:0.7   | 250                       | 22            | 120 ± 25              | 1.0             | 663                                    | 109   | 0.63                                   | 2.7                  |
| <b>AR2</b>    | 0.2:1000:5:0.7   | 230                       | 22            | 77 ± 9 × 198 ± 53     | 2.5             | 443                                    | 102   | 0.59                                   | 2.7                  |
| <b>AR4</b>    | 0.4:1000:10:1.4  | 350                       | 22            | 159 ± 49 × 594 ± 82   | 3.8             | 1191                                   | 231   | 1.17                                   | 2.8                  |
| <b>AR8</b>    | 0.4:1000:10:1.4  | 250                       | 22            | 136 ± 26 × 1028 ± 139 | 7.6             | 284                                    | 47  | 0.26                                   | 2.7                  |

\* Data were mean ± SD (n = 3).

<sup>#</sup> Based on theoretical calculation as shown in Supplemental Calculation 1.

**Table 2**

Hydrodynamic size and surface charge of SiO<sub>2</sub> before and after primary amine modification in aqueous suspension at pH 7.0.\*

|               | Before APTES modification |                     | Post APTES modification |                     |
|---------------|---------------------------|---------------------|-------------------------|---------------------|
|               | Size by DLS (nm)/PDI      | Zeta potential (mV) | Size by DLS (nm)/PDI    | Zeta potential (mV) |
| <b>Stöber</b> | 148.0 ± 0.4/0.043         | -50.4 ± 1.0         | 174.2 ± 1.9/0.102       | 17.0 ± 0.7          |
| <b>Meso S</b> | 257.8 ± 0.9/0.219         | -39.4 ± 0.5         | 233.8 ± 2.2/0.145       | 32.4 ± 0.9          |
| <b>AR2</b>    | N/A                       | -33.5 ± 0.5         | N/A                     | 32.0 ± 1.0          |
| <b>AR4</b>    | N/A                       | -34.0 ± 1.2         | N/A                     | 40.3 ± 1.0          |
| <b>AR8</b>    | N/A                       | -36.6 ± 0.6         | N/A                     | 36.7 ± 0.5          |

\* Data were mean ± SD (n = 3).



**Table 3**

Summary of IC<sub>50</sub> values of SiO<sub>2</sub> on RAW 264.7 macrophages.\*

| IC <sub>50</sub> values (µg/mL) | Stöber   | Meso S   | AR2     | AR4      | AR8      |
|---------------------------------|----------|----------|---------|----------|----------|
| Bare nanoparticles <sup>#</sup> | 73 ± 3   | 89 ± 4   | 72 ± 12 | 92 ± 6   | 74 ± 18  |
| Amine-modified nanoparticles    | 254 ± 15 | 182 ± 38 | 471 ± 7 | 184 ± 17 | 225 ± 28 |

\* Data were mean ± SD (n = 3).

<sup>#</sup> There was no significant difference in IC<sub>50</sub> among all types of bare SiO<sub>2</sub> ( $p > 0.05$ ), however, statistically significant differences were observed between IC<sub>50</sub> of each type of bare SiO<sub>2</sub> and that of their amine-modified counterparts ( $p < 0.001$ ).

**Table 4**

Average cellular association of bare SiO<sub>2</sub> detected by ICP-MS on RAW 264.7 post incubating with nanoparticles at 100 μg/mL for 24 hours.\*

| Nanoparticle treatment | Silicon content (μg)/100 μg protein | No. nanoparticles/100 μg protein |
|------------------------|-------------------------------------|----------------------------------|
| Stöber                 | 21.2                                | $2.6 \times 10^{11}$             |
| Meso S                 | 0.7                                 | $1.6 \times 10^{10}$             |
| AR2                    | 0.8                                 | $2.2 \times 10^{10}$             |
| AR4                    | 0.5                                 | $1.8 \times 10^9$                |
| AR8                    | 0.5                                 | $6.1 \times 10^8$                |

\* There was no significant difference in the amount of cellular associated silicon content per 100 μg protein among various types of mesoporous SiO<sub>2</sub> ( $p > 0.05$ ). Stöber nanoparticles were associated with RAW 264.7 at significantly higher levels than mesoporous SiO<sub>2</sub> of all types either in mass concentration or in number concentration ( $p < 0.001$ ). Data were mean of triplicates.

**Table 5**

Summary of LC<sub>10</sub> values of SiO<sub>2</sub> in human erythrocytes.\*

| LC <sub>10</sub> values (µg/mL) | Stöber | Meso S  | AR2     | AR4     | AR8     |
|---------------------------------|--------|---------|---------|---------|---------|
| Bare nanoparticles <sup>#</sup> | 36 ± 1 | 154 ± 4 | 115 ± 1 | 152 ± 2 | 302 ± 3 |
| Amine-modified nanoparticles    | 97 ± 4 | 30 ± 1  | 40 ± 1  | 23 ± 1  | 43 ± 1  |

\* Data were mean ± SD (n = 3).

<sup>#</sup> There was significant difference between the LC<sub>10</sub> value of bare SiO<sub>2</sub> and that of amine-modified counterparts ( $p < 0.001$ ).